Photonic crystal fiber in the polychaete worm *Pherusa* sp.

Tomasz M. Trzeciak* and Peter Vukusic†
Electromagnetic Materials, School of Physics, Exeter University, Exeter EX4 4QL, United Kingdom
(Received 21 July 2009; published 14 December 2009)

Setae of the polychaete worm *Pherusa* exhibit remarkably strong photonic effects, which arise from their two-dimensional-periodic internal structure of hexagonally packed cylindrical channels. The hexagonal order is limited to monocrystalline domains of different orientation, which results in an overall polycrystalline effect. A detailed experimental and theoretical investigation of this structure reveals that the internal photonic structure is carefully tuned with respect to its lattice constant in order to provide an optical response coinciding with the visible wavelength rage. A further optimization is observed for the packing fraction of cylindrical channels in order to maximize the width of photonic band gaps, and hence the reflectance of incident visible light.

DOI: 10.1103/PhysRevE.80.061908 PACS number(s): 87.90.+y, 42.70.Qs

I. INTRODUCTION

Structural color in natural systems such as in Insecta, Aves, and marine animals, results from an interaction of light with nanostructures having periodically ordered refractive index variations in one-dimensional (1D), two-dimensional (2D), or three-dimensional (3D) geometries [1]. The significance of these naturally grown photonic systems has extended beyond the bioscience communities. They have generated interest in mainstream photonic physics communities because of the increasing importance of photonic band gap materials to light manipulation technologies [2].

Natural systems exhibiting 1D periodic nanostructure are relatively common and have been well documented [3–5]. They typically give rise to characteristic optical multilayer phenomena [3] and fulfill various biological functions, usually related to appearance [3,6]. 3D periodic natural animate and inanimate systems have also been the subject of numerous detailed investigations [4,7–10]. In contrast, however, natural systems, which exhibit 2D periodicity, are less common and have therefore been the subject of far fewer thorough investigations. Indeed, few truly 2D natural photonic systems have been documented at all. The exception to date is that of the polychaete worm *Aphrodite*, the setae of which can be up to approximately 1 cm in length and which comprise many hundreds of closed-packed hollow channels that run longitudinally through each seta [6,11–13]. Another polychaete worm, *Pherusa* sp., is also known to exhibit analogous photonic nanostructure in its setae, but with periodicity extending over a larger length scale [4]. Although its structure has been documented, it was not the subject of a systematic structural and photonic investigation. Our work here sets out to complete this investigation for the structurally colored 2D periodic system of *Pherusa* sp. setae via an experimental and theoretical investigation. Detailed experimental measurement of its photonic properties, statistical analysis of a large sample number of setae cross sections and subsequent theoretical modeling of the revealed internal structure are reported.

*t.m.trzeciak@ex.ac.uk
†p.vukusic@ex.ac.uk; http://newton.ex.ac.uk/research/emag

II. EXPERIMENTAL MATERIALS AND METHODS

Representative samples of *Pherusa* polychaete worm were acquired from the collection at the Royal Albert Museum, Exeter, and the Australian Museum, Sydney. The internal structure of the setae from these samples was investigated by transmission electron microscopy (TEM) using a JEOL 100S TEM. TEM images were taken after fixing the samples in 3% glutaraldehyde at 21 °C for 2 h followed by rinsing in sodium cacodylate buffer. Samples were then fixed in 1% osmic acid in buffer for 1 h followed by block staining in 2% aqueous uranyl acetate for 1 h, dehydration through an acetone series ending with 100% acetone and embedding in Spurr's resin [14]. Series of 1 cm long setae were sectioned at 2 mm intervals along their length using a Boeckeler PowerTome-PC microtome with a Drukker diamond knife as the cutting blade. Each section was (70 ± 10) nm thick. Post microtomed sample sections were stained with lead citrate.

Optical microscopy examination of individual setae samples immersed in deionized water was performed in reflection, under bright field polarized and unpolarized illumination, using a Carl Zeiss Axioskop 2 polarizing microscope (Imaging Associates, Cambridge, U.K.). Images were acquired using a high-resolution AxioCam MRc5 digital camera.

Reflectance spectra were collected through an optical fiber (Ocean Optics P1000–2-UV/Vis) mounted on the optical microscope's eyepiece and connected to an Ocean Optics USB4000 UV-Vis-IR spectrometer. The iris of the microscope located in the image plane was adjusted to make the size of the probed sample region comparable to the diameter of the setae. The acquired spectra were corrected for dark current and normalized with respect to a white spectrum reference obtained from a Labsphere certified reflectance standard. This removes the characteristic spectral profile of the incident light source, however, due to the diffuse reflectance of the reference surface the normalization is to an arbitrary intensity.

Three-dimensional optical scattering data through the setae cross sections were acquired using a Leica TCS SP5 scanning confocal microscope. Series of images were acquired at different focal depths, from which three-dimensional representations of each observed region were reconstructed using IMAGEJ software package [15]. This pro-

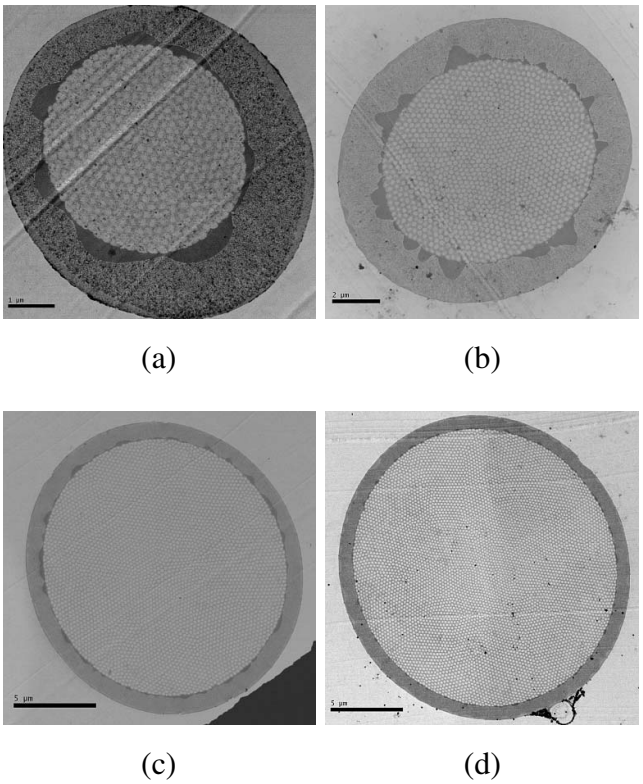

FIG. 1. TEM images of selected cross sections at different locations along iridescent setae from *Pherusa*; scale bars: (a) 1 μm, (b) 2 μm, (c) 5 μm, and (d) 5 μm.

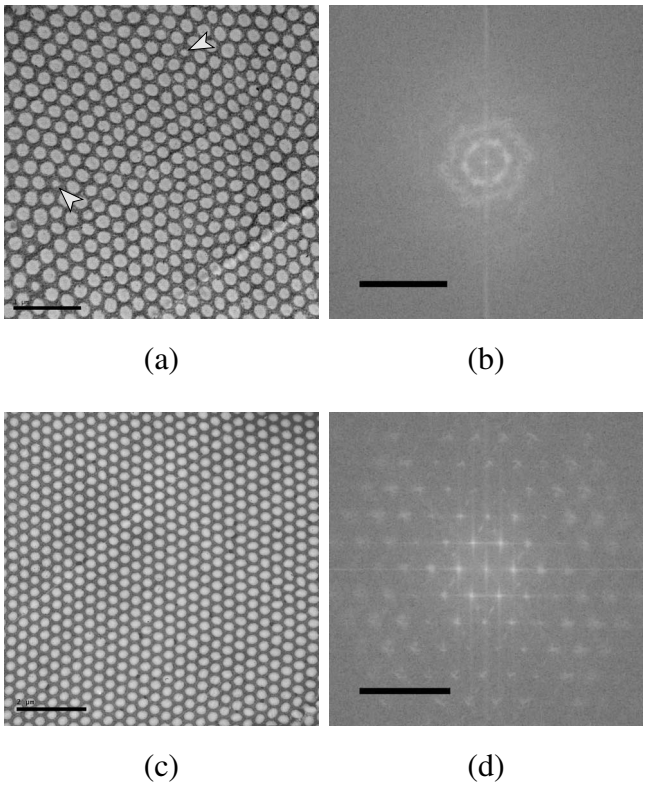

FIG. 2. TEM images of cross sectional regions from *Pherusa* setae (left) and their FFT (right). This study (top), Vukusic and Sambles [4] (bottom); scale bars: (a) 1 μm, (b) 20 μm^{-1}, (c) 2 μm, and (d) 10 μm^{-1}. Arrows mark the terminal points of the hollow tubular fibrils.

cedure was repeated for illumination with three different wavelengths (458, 514, and 633 nm) from the light sources integrated within the confocal system. The images for these three wavelengths were then combined into the final false color RGB image.

III. RESULTS

A. Internal structure of *Pherusa* setae

The investigated samples of setae were removed at the base from a *Pherusa* specimen. Their length was (0.90 ± 15) cm and the diameters were in the range of a few tens of micrometers depending on the distance from their proximal tip. The underlying internal structure of these setae consists of hollow tubular fibrils formed from sclerotized chitin [13,16] and running lengthwise along the seta in closed packed domains of hexagonal order. At the edge, this ordered structure is surrounded by an approximately 1 μm-thick layer of homogeneous material (Fig. 1).

These hollow cylindrical channels are packed into "monocrystalline" domains of different orientation [Figs. 1 and 2(a)], giving rise to an overall polycrystalline effect. This can be observed in the fast fourier transforms (FFT) of the TEM images that show the ring-like diffraction patterns normally associated with polycrystalline structures [Fig. 2(b)]. This domained setae structure is in contrast with the earlier preliminary studies of a different *Pherusa* species [4], for which nearly perfect monocrystalline arrangements of channels are observed almost throughout the entire cross section. An example of this is shown in Figs. 2(c) and 2(d) with cross sectional region and its FFT, respectively. The difference is believed to be a subspecies related effect.

Detailed investigation of the domained structure of these setae was performed by statistical analysis of cross sectional images from 50 different setae sections.

Image analysis of each seta cross section was performed in several steps. First, images were converted into binary black and white masks that discriminate cylindrical channels from the setae material. To this end each image was prefiltered to remove high frequency noise and subsequently thresholded to obtain the final black and white mask.

Thresholding is typically done by choosing a fixed value of gray level that discriminates between white and black regions. This method, however, proved to be unreliable and prone to artifacts, such as merging of different channels together. Therefore, instead of using a constant gray level, thresholding was done with gray level masks produced by oversmoothing the images themselves.

The regions of connected pixels on processed black and white images were subjected to granulometry measurements. The position (centroid), size (area-equivalent diameter) and ellipticity of each region was obtained in this step. Regions close to image borders and resulting from artifacts were excluded from the analysis to avoid biasing. Additionally, Delaunay triangulation of regions' centroids was performed to

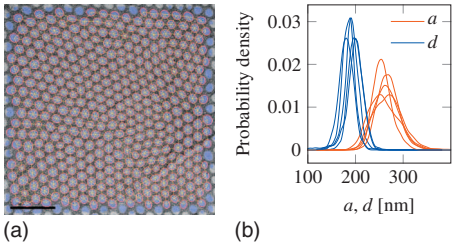

FIG. 3. (Color) Image analysis of cross sections from *Pherusa* setae: (a) TEM image with the effect of image thresholding (blue), granulometry (red) and Delaunay triangulation (yellow), scale bar 1 μm; (b) distributions of channel sizes, d, and center-to-center distances, a, for 5 representative cross sections.

obtain cylinders' center-to-center distances (taken as a measure of the structure's lattice constant). The effect of this multistep procedure is illustrated in Fig. 3(a).

The data obtained from the above described image analyses provide a broad range of statistical information about the internal structure of *Pherusa* setae. In Fig. 3(b), typical distributions of center-to-center distances between channels, a, and their diameters, d, are shown. Generally, these distributions are fairly narrow with standard deviations being less than 10% of the mean value. The shape of the channels is close to circular with the mean aspect ratio of the fitted ellipses being equal to 1.25 ± 0.17.

The mean values of the channel diameter and interchannel distance obtained for 50 different setae cross sections are proportional to each other with a high degree of correlation (correlation factor $R=0.95$, the highest value of all relations investigated in this study). The proportionality relation between the channel size and the lattice constant is further corroborated by the fact that the packing fraction of channels, ϕ, (and therefore also the ratio of the channel size to lattice constant) remains approximately constant and is equal to 0.47 ± 0.06, regardless of the distance from the proximal tip of the seta.

The mean channel size and lattice constant associated with the cross-sectional structure of setae show an approximately linear dependence on the setae diameter, D. Figure 4 shows linear fits to both data sets (solid lines) together with 95% confidence envelope of the fitted lines (dashed lines). The nonvanishing constant terms present in those fits (122

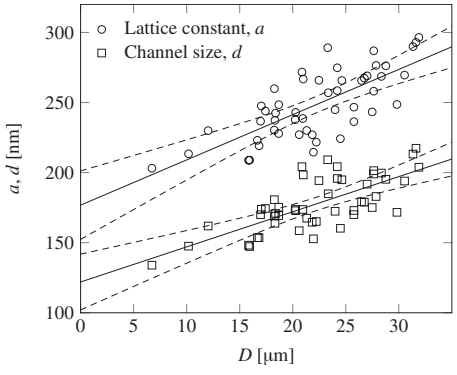

FIG. 4. Photonic structure lattice constant, a, and channel size, d, as a function of the seta diameter, D.

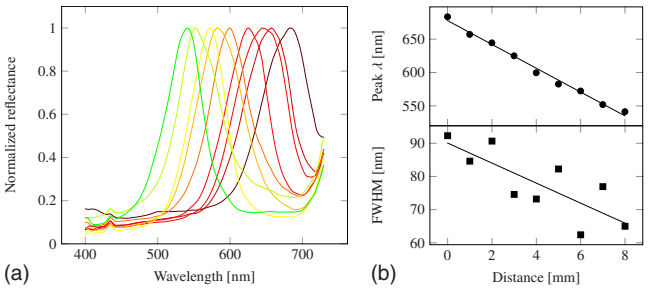

FIG. 5. (Color online) Reflectance spectra for translation along the seta at 1 mm intervals: (a) reflectance spectra, (b) wavelength of the peak reflectance (top) and full width at half maximum (FWHM) of the spectra (bottom).

nm for channel size and 177 nm for lattice constant) imply that the internal structure of the setae is not simply rescaled in proportion to its diameter. In fact, as each seta becomes thinner toward its distal tip, not only do the channel size and lattice constant decrease but also the number of channels reduces as some of them terminate along the fiber. Two such terminal points of the channels are marked with arrows in Fig. 2(a).

B. Optical measurements

The optical response of *Pherusa* setae to incident light was measured in a number of experiments following the procedures described in Sec. II. First, the change in the reflectance spectra as a function of the position along individual setae was investigated. Spectra were acquired along many individual setae with approximately 1 mm separation between the probed regions starting from the proximal end. Representative spectra from one set of such measurements are shown in Fig. 5(a). As the acquisition point moves from the proximal end of the seta toward its distal end, the peak reflectance of the spectrum shifts from 680 to 540 nm, respectively in almost linear fashion as shown in the top graph of Fig. 5(b). A similar decrease is observed for the full width at half maximum (FWHM) of the spectrum (from 85 to 65 nm) but there is considerably more variability present in this quantity [Fig. 5(b), bottom graph].

Whether the reflectance spectra depend on the polarization of incident light was examined by acquiring spectra along individual setae, with setae aligned parallel and perpendicular to the polarization axis. For each location along the seta two sets of spectra were acquired: with polarized and with unpolarized illumination. Negligible difference between either equivalent set of polarization data was observed.

Further investigation of variation in the profile of the reflectance spectra was performed by acquiring several spectra at the same location along the seta but at different angles of rotation about its longitudinal axis changing in steps of a few tens of degrees (Fig. 6). There is some variation in the reflectance profile with the rotation angle, although the range of wavelengths that are strongly reflected remains approximately constant with peak reflectance around 560 nm for this region of the seta. Optical microscope images corresponding to these spectra are also shown in Figs. 6(a)–6(c). One can

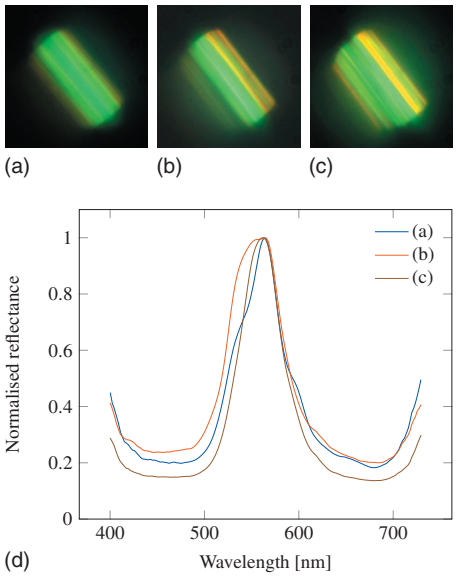

FIG. 6. (Color) Reflectance spectra at different rotation angles of *Pherusa* seta about its longitudinal axis together with the corresponding optical microscope images showing distinct color transition across seta's width.

observe that iridescent color appears rather uniform longitudinally along the seta but there are some distinct color transitions across its width.

Additional measurements of optical scattering from the internal structure of the setae were performed using scanning confocal microscopy. Using this technique it was possible to reconstruct three-dimensional images from the two-dimensional planes taken at a resolution of 320 nm step sizes through the structure. The reconstructed images for three chosen wavelengths of incident light were combined into a false color RGB image, with blue, green and red color channels corresponding to scattering of 458, 514, and 633 nm monochromatic illumination, respectively (Fig. 7). Domains of strong colored reflection in these reconstructed cross sections are clearly distinguishable and arise from the different

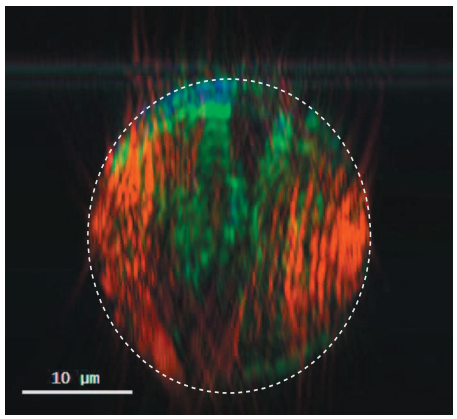

FIG. 7. (Color) Cross sectional view of scattering from a *Pherusa* seta reconstructed from scanning confocal microscopy measurements. RGB color channels correspond to scattering measured for three chosen incident wavelengths: 458 nm (blue), 514 nm (green), and 633 nm (red).

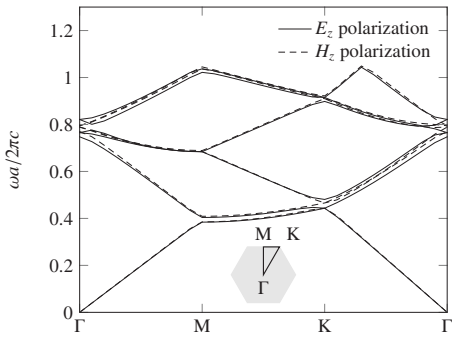

FIG. 8. Photonic band diagram for hexagonal lattice of channels (packing fraction of channels ϕ=0.47, refractive index ratio 1.56/1.33); boundary of the first Brillouin zone is shown on the inset.

orientation of the closed-packed channel domains within the seta.

C. Computational modeling

Finite element model (FEM) analysis of the *Pherusa* setae internal structure were performed using COMSOL MULTIPHYSICS™ software package with rf module [17]. The geometry of the structure was modeled as a hexagonal unit cell with a circular central channel and Floquet boundary conditions at the edges. The size of the central channel was chosen such that the packing fraction of channels matches the value of 0.47 found for the structures analyzed in Sec. III A.

The refractive index of tissue constituting the walls of setae internal channels is difficult to establish but it can be expected in the range of 1.54–1.57 [12,18]. For our calculations values of n_1=1.56 and n_2=1.33 were assumed for the channel walls and water filled interior of the channels, respectively. Optical absorption in the setae, inferred to be largely absent based on visual comparisons with other well documented natural samples [19], was assumed negligible.

Photonic band diagrams obtained from the eigenvalues of the FEM model of the setae intradomain structure are shown in Fig. 8, where the reduced frequency, $\frac{\omega a}{2\pi c}$, of the lowest 6 bands is traced along the boundary of the first Brillouin zone. No full photonic band gap is observed for either of the polarizations for the chosen model parameters, however, partial band gaps exist in $\Gamma-M$ and $\Gamma-K$ directions (Table I).

The band structure is largely insensitive to the shape of the central channel. This was assessed by calculations for elliptical channels of aspect ratio up to 1.6 while maintaining constant packing fraction of 0.47. No significant changes in band positions were discerned.

Changes in the packing fraction of channels, however, have much bigger impact on the photonic band structure. The

TABLE I. Reduced frequencies, $\frac{\omega a}{2\pi c}$, of the lowest bandgaps for hexagonal lattice of channels; packing fraction of channels ϕ =0.47, refractive index ratio 1.56/1.33.

Polarization	$\Gamma-M$	$\Gamma-K$
E_z	0.384–0.404	0.443–0.481
H_z	0.385–0.409	0.444–0.466

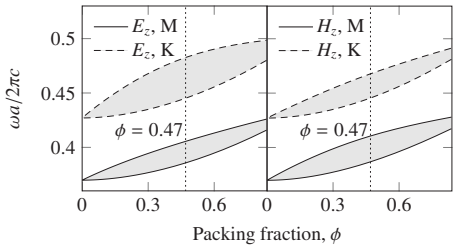

FIG. 9. The lowest eigenfrequencies on the band diagram, which demarcate the local stop gaps (shaded regions) as a function of channel packing fraction, ϕ, for E_z (left pane) and H_z (right pane) polarizations; refractive index ratio 1.56/1.33.

central frequencies of the band gaps in the $\Gamma-M$ and $\Gamma-K$ directions increase with increasing packing fraction of channels as shown in Fig. 9. Furthermore, the frequency intervals of these band gaps exhibit a maximum width at some specific packing fraction. The value of the packing fraction that maximizes the band gap depends on the refractive index contrast of the photonic structure. This is shown in Fig. 10, where the band-gap-maximizing packing fraction is plotted as a function of refractive index of the channel wall material. It can be observed that with increasing magnitude of the refractive index of the channel wall material, n_1, maximal band gaps occur for higher packing fractions. The mean packing fraction obtained from the image analyses of 50 *Pherusa* setae cross sections is $\phi=0.47$ and is indicated in Fig. 10 with 95% confidence interval as shaded region.

Figure 11 shows the calculated reflectance spectra for both polarizations and for *M* and *K* high symmetry points for 32 lattice layers of cylindrical channels using $n_1=1.56$ and $\phi=0.47$. The shape of those spectra is reminiscent of that from multilayered structures [3]. Reflectance is close to 100% for this number of lattice layers. There is also a considerable overlap of spectra for the E_z and H_z polarizations but there is essentially no overlap for two high symmetry points (hence, the lack of full and complete band gap). The central frequencies and the widths of the reflected frequency ranges are in agreement with those obtained from the band diagram calculations.

IV. DISCUSSION

The photonic structure present inside of *Pherusa* setae appears similar to that of *Aphrodite*. However, there are

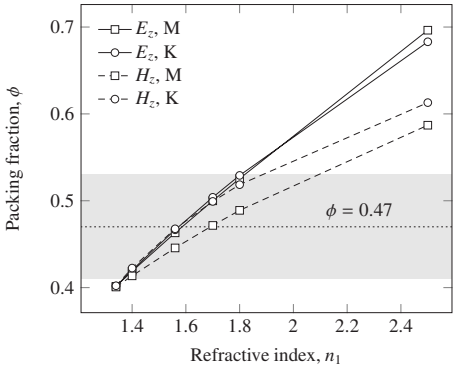

FIG. 10. Channel packing fraction, ϕ, as a function of channel wall refractive index, n_1 ($n_2=1.33$).

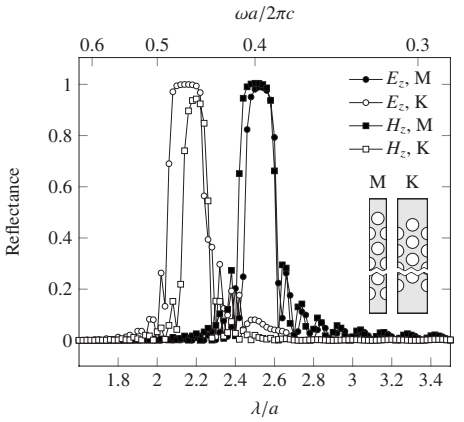

FIG. 11. Calculated reflectance spectra from 32 lattice layers of channels with model geometries on the inset; packing fraction of channels $\phi=0.47$, refractive index ratio 1.56/1.33.

some notable differences. For the samples of *Pherusa* species investigated in this study the pitch of the photonic structure was in the range of 200–300 nm, which is significantly lower than the value of 520 nm reported for *Aphrodite* [12,13]. As a result the iridescence of *Pherusa* setae in the visible wavelength range originates from the lowest frequency band gaps as opposed to higher frequency band gaps in case of *Aphrodite*.

Hollow tubular fibrils constituting the structure of *Aphrodite* setae vary in diameter across the cross section, with the largest ones being located in the seta's center and gradually decreasing toward the edges, while the lattice constant of the structure remains the same throughout the cross section. Setae of *Pherusa* do not exhibit such a variation and the pitch as well as the packing fraction of the hexagonal structure is the same across the entire cross section. Furthermore, the packing fraction remains approximately constant also along the setae length and only the lattice constant gradually decreases toward each seta's distal tip. However, this reduction in the pitch size of the structure is not proportional to the accompanying reduction in the seta diameter. All the measured pitch sizes fall within the range of 200–300 nm. If this range is used to recalculate the reflectance spectra from Fig. 11 in the absolute units, it becomes apparent that this variation in the lattice constant magnitude leads to an optical response covering almost the complete range of the visible wavelengths—an observation that is also confirmed by the experimentally acquired reflectance spectra.

Given the fact, that the packing fraction and the refractive index of the photonic structure can be considered constant, the optical response of the structure is determined solely by its lattice constant. An increase in the pitch size will induce a proportional increase in the peak reflectance of the spectrum as well as its width. Indeed, such a proportionality between the shift of the peak reflectance and FWHM of the spectrum was observed experimentally, cf. Figure 5(b).

Another intriguing aspect uncovered in this study is the overall polycrystalline nature of the photonic structure of *Pherusa* sp., something that seems to be absent from other polychaete worms analyzed to date [4,12]. The emergence of such a polycrystalline structure could be possibly explained

by the creation of local defects in the lattice at the termination points of tubular fibrils, defects which in turn require local rearrangement of the fibrils in order to maintain closed packed configuration. Maintaining a strictly periodic arrangement of the channels beyond a certain length does not improve the optical response any further. In our simulations, approximately 30 lattice periods were sufficient to achieve nearly 100% reflectance, while the observed effective number of lattice layers in the analyzed samples varied from 20 to over 100 depending on seta diameter. One could speculate about the role served by this domaining of the structure to be the orientational averaging of the structure's optical response, however, without additional investigation it is difficult to determine this conclusively.

The width of the reflectance spectrum is contained well within the range spanned between the lowest band gaps calculated for the two high-symmetry points of the hexagonal lattice. For example, for the E_z polarized incident light and a lattice constant equal to 250 nm—a typical value for our specimen—the central wavelength of the band gap shifts from 540 nm at the K-point to 635 nm at the M-point. This is in accordance with the spread of the measured spectra shown in Fig. 5 and 6, as well as with the predominant scattering of the green-red wavelengths observed in Fig. 7. The actual polarization of the incident light has essentially no impact on the reflectance, an effect that was observed experimentally and that can be readily understood based on a significant overlap between the reflectance spectra obtained for the two polarizations as shown in Fig. 11.

The strongest optical response of the photonic structure, such as the one found in the polychaete worm *Pherusa*, can be expected when the width of the frequency stop gaps has the largest magnitude. Given the limited range of refractive index contrast that can be achieved in natural systems, the only other parameter suitable for optimization is the structure's packing fraction. It was found that for the packing fraction obtained from the image analyses, $\phi=0.47\pm0.06$, the band gaps of maximum width occur for the refractive index of the structure equal to approximately 1.6. This value is remarkably close to the values used in the literature for similar structures, which provides a strong indication that the packing fraction of cylindrical channels in *Pherusa* setae is optimized for the maximum reflectance.

V. CONCLUSIONS

In this study, we presented a detailed experimental and theoretical investigation of the structurally colored setae of the polychaete worm *Pherusa*. Like the related *Aphrodite* system, *Pherusa* setae exhibit remarkably strong photonic effects which arise from their 2D-periodic internal structure. This structure consists of hollow cylindrical channels running lengthwise and closed packed in domains of hexagonal order. These domains, in turn, form an overall polycrystalline structure.

The packing fraction of tubular fibrils remains approximately constant throughout the entire setae, while the pitch of the hexagonal structure decreases as each seta becomes thinner toward its distal tip. This change in lattice constant of the structure is not proportional to the change in the seta diameter, but rather it is optimized to give the strongest optical response that coincides with the visible wavelength range.

Further optimization of this natural 2D photonic structure occurs for the packing fraction of the cylindrical channels. Based on systematic image analyses of TEM micrographs of seta sections and theoretical modeling of the structure it was found that the packing fraction of 0.47 ± 0.06 maximizes the width of partial photonic band gaps and, therefore, also maximizes the range of strongly reflected wavelengths.

[1] S. Kinoshita and S. Yoshioka, *Structural Color in Biological Systems—Principles and Applications* (Osaka University Press, Osaka, Japan, 2005), pp. 153–176.
[2] J. D. Joannopoulos, S. G. Johnson, J. N. Winn, and R. D. Meade, *Photonic Crystals: Molding the Flow of Light (Second Edition)* (Princeton University Press, Princeton, NJ, 2008).
[3] M. F. Land, Prog. Biophys. Mol. Biol. **24**, 75 (1972).
[4] P. Vukusic and J. R. Sambles, Nature (London) **424**, 852 (2003).
[5] A. R. Parker, in *Functional Morphology of the Invertebrate Skeleton*, edited by E. Savazzi (Wiley, Chichester, 1999), pp. 65–90.
[6] H. M. Fox and G. Vevers, *The Nature of Animal Colours* (Sidgwick and Jackson Ltd., London, 1960).
[7] V. L. Welch and J. P. Vigneron, Opt. Quantum Electron. **39**, 295 (2007).
[8] R. B. Morris, Journal of Entomology Series A: Physiology and Behaviour **49**, 149 (1975).
[9] J. W. Galusha, L. R. Richey, J. S. Gardner, J. N. Cha, and M. H. Bartl, Phys. Rev. E **77**, 050904(R) (2008).
[10] K. Michielsen and D. G. Stavenga, J. R. Soc., Interface **5**, 85 (2008).
[11] W. Schmidt, Giessener Naturw. Vortr. **6**, 30 (1949).
[12] A. R. Parker, R. C. McPhedran, D. R. McKenzie, L. C. Botten, and N. A. P. Nicorovici, Nature (London) **409**, 36 (2001).
[13] R. C. McPhedran, N. A. Nicorovici, D. R. McKenzie, L. C. Botten, A. R. Parker, and G. W. Rouse, Aust. J. Chem. **54**, 241 (2001).
[14] A. R. Spurr, J. Ultrastruct. Res. **26**, 31 (1969).
[15] http://rsbweb.nih.gov/ij/index.html.
[16] D. E. G. Briggs and A. J. Kear, Paleobiology **19**, 107 (1993).
[17] http://www.comsol.com.
[18] V. Welch, J. P. Vigneron, V. Lousse, and A. Parker, Phys. Rev. E **73**, 041916 (2006).
[19] P. Vukusic (unpublished).